Wind Turbine Team at Virginia Tech

Technical Design Written Report

2020 U.S. Department of Energy Collegiate Wind Competition

Virginia Tech

Blacksburg, Virginia, (540) 231-6611, WindTurbineTeamVT@vt.edu
Twitter/Instagram/Facebook: @WindTurbineTeamVT

Team Leaders

Jonathan Hawes (Technical Lead & Project Manager) | **Alvaro Armaza** (Project Manager)
Katie Clatterbuck (Siting & Business) | **Sean Simpson** (Mechanical)
Cole Casteel (Power Systems and Controls) | **Zach Fink** (Blades)

Advisors

Dr. Matthew Kuester (Principal Investigator, Department of Aerospace Engineering)
Dr. Arthur Ball (Assistant Investigator, Department of Electrical and Computer Engineering)

Members: 53 (8 majors), Advisors: 2

COLLEGIATE WIND COMPETITION
U.S. DEPARTMENT OF ENERGY

VIRGINIA TECH

Table of Contents

Executive Summary

Following the success of our 2019 competition turbine, the Wind Turbine Team at Virginia Tech sought to improve upon the failures of the previous year's design as opposed to redesigning the entire turbine. This approach allowed the team to maintain the sub-systems that had proved successful while addressing the main concerns and shortcomings from the competition. In using this approach, the team focused on three design principles that guided the entire system: safety, reliability, and innovation. For systems that had failed the previous year in some capacity, addressing safety was the highest priority. For systems that had were successful in last year's design, improving reliability was necessary to ensure successful performance during testing. Finally, to improve upon existing systems, the team focused on finding innovations that would improve the performance of the turbine.

As addressing the safety of the turbine was the team's first concern, the team focused on systems that would directly impact the Safety and Cut-out tasks of the competition. The team added a mechanical brake to the drive system, in addition to an existing pitch control and drive system, such that the turbine could be stopped completely during unsafe operating conditions and be able to restart as soon as possible. The team also reinforced the hub of the turbine to prevent destructive failures that had occurred in previous years such that the hub could withstand the intensely high forces experienced during the Cut-out task. In addition, the team explored material changes to sub-systems such as the blades to reduce the weight and improve the strength of the sub-system.

To improve the reliability of the turbine, the team sought to improve the control of the turbine and its sub-systems. The load design was changed to a combination of a battery and a resistor such that any necessary sub-system would be able to draw power from the load when the turbine was unable to provide enough power. The team also planned to implement most of the electronics with printed circuit boards to increase the reliability with which all electronic systems could be both manufactured and operated.

Finally, the team sought innovations with respect to the aerodynamic design of the blades and the electrical system. After the successful performance of the previous year's blades, the team researched how the addition of winglets could improve the power performance of blades that already met most of the team's criteria. In addition, the team sought to maximize the efficiency of the turbine through the development of a maximum power-point tracking system.

Although the turbine in its full design, shown partially in **Figure 1**, could not be tested because of the COVID-19 pandemic, the Wind Turbine Team at Virginia Tech is confident in its design. The design approaches taken allowed the team to take an already successful turbine design and improve upon it in such a way that would allow the turbine to perform well in all tasks of the Collegiate Wind Competition.

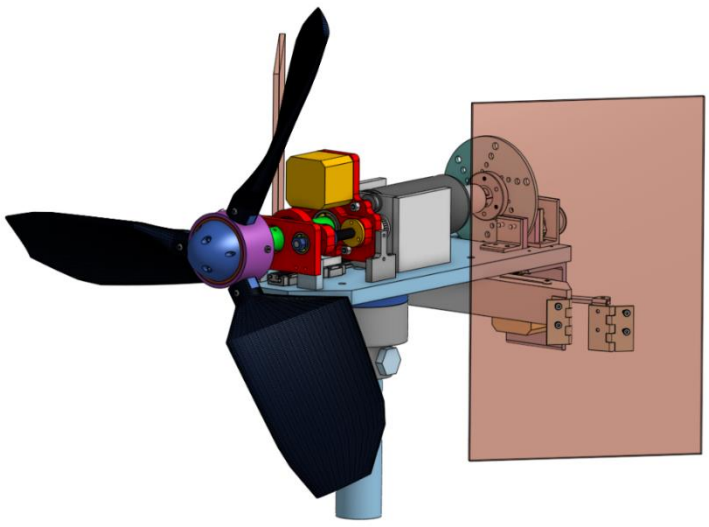

Figure 1. Partial CAD Model of Turbine, showing a double-tail design.

Blades

Blade Design

The Aerodynamics Sub-Team designed the blades to build off the success of the previous year's blades while exploring innovative technologies to improve aerodynamic performance. The team focused on the addition of winglets to the tips of the blade. While there was not an opportunity to collect significant data on blade performance, two prototypes were developed. Our plan was to take off one centimeter from the tip of last year's blade design blade and replace it with one-centimeter winglets. Once the winglets are glued on the tip of the blade, our strategy was to compare the cut-in and maximum power generation across a variety of windspeeds.

Airfoil Selection

Airfoil selection is crucial to balance both low and high wind speed performance. The root of the blade has a greater influence at low wind speeds and cut-in performance while the tip of the blade influences high wind speed and rated power performance. A two-airfoil design was thus chosen to maximize blade performance at both cut-in wind speed and rated power. A variety of airfoils were analyzed in XFOIL across the expected Reynolds number range to determine the best performing airfoils. The FX 63-137 was chosen as the root airfoil because its high lift coefficient improves cut-in and the SG6043 was chosen as the tip airfoil because its high lift to drag ratio improves overall power performance. The middle section of the blade is a gradual linear spline between the two airfoils to smooth out aerodynamic discontinuities that would be present from sudden changes in cross section. The two airfoils used in the design can be seen in **Figure 2**. As verification of our decision to use two airfoils spliced together, our optimization code, explained in the following section, was run to analyze the performance of a singular airfoil, both the FX 63-137 and the SG6043 alone, and as a combination of the two airfoils. The combination of the two airfoils proved to perform significantly better in both cut-in and power distribution across all competition wind speeds.

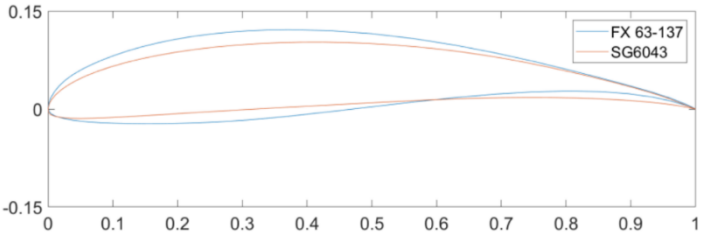

Figure 2. Cross section for FX 63-137 and SG6043 airfoils.

Chord and Twist Design

The Aerodynamics Team developed multiple in-house MATLAB programs to allow for a more customizable design process compared to using externally available open-source code. Chord and twist designs were initially completed in MATLAB and finalized using QBlade, an open sourced program that analyzes blades given the input of a rotor table. First, the team developed a Blade Element Momentum Theory (BEMT) code in MATLAB.[1,2,3,4] In combination with the BEMT code, an optimization code[5] was created to determine the initial chord and twist distribution of the blade. The user specifies multiple parameters including an initial blade design to be optimized, any desired geometric constraints on the design, and the optimization objective: minimize cut-in wind speed, maximize power curve performance, or both. The code goes through a numerically implemented gradient based optimization algorithm to find the design that maximizes the points as described by the competition. The optimization code was run several times to account for various combinations of cogging torque and initial chord/twist distribution, and the chord and twist design that yielded the maximum competition points was selected. The algorithm determined that a long chord starting at the root airfoil and gradually tapering towards the tip of the blade resulted in a similar power curve but better cut-in. **Figure 3** shows the final chord and twist distribution that includes the cylindrical and airfoil portions of the blade.

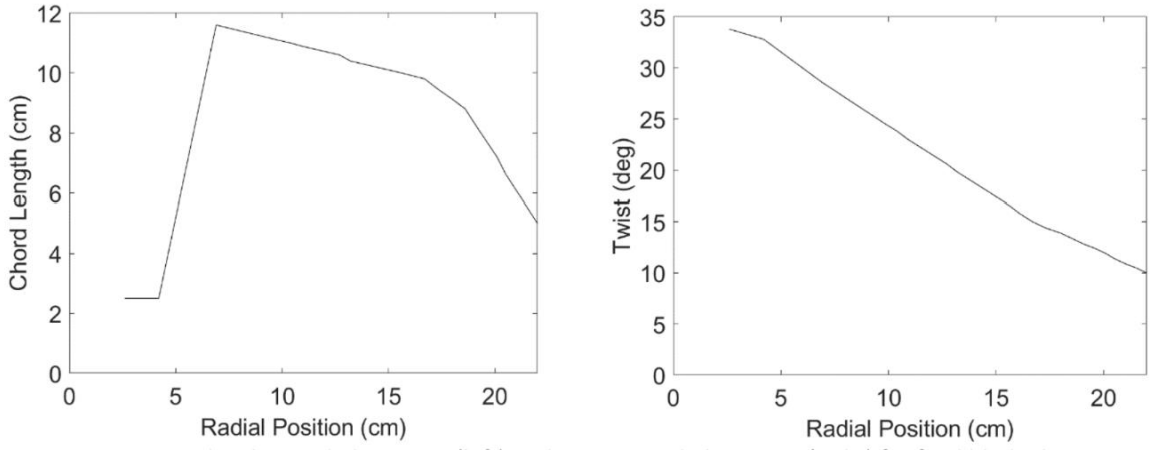

Figure 3. Chord vs. radial position (left) and twist vs. radial position (right) for final blade design.

The output of the optimized geometry was sent into QBlade to incorporate the cylindrical region near the root and smooth out any geometric transitions. **Figure 4** shows the final blade design.

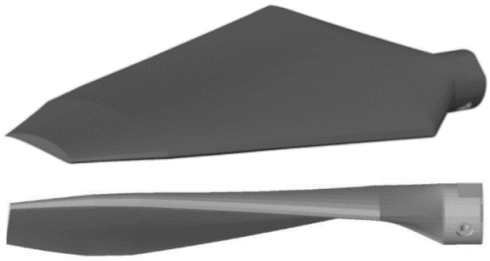

Figure 4. 3D model of the final blade design.

Blade Performance

While aerodynamic analysis could have been performed with the team's in-house MATLAB code, QBlade was ultimately used because of advanced features such as interpolated airfoil data for splined sections, new tip and root loss corrections, and 3D corrections. Blade power curves were generated using two different generator loads. These blade power curves are represented by the solid lines in **Figure 5**. These curves show the importance of selecting the appropriate generator load to best match the blade power curves, which is discussed in the Power Systems and Controls section. Using this graph, we can show that the blades could provide enough torque to overcome the generator and spin the turbine at low wind speeds. It is important to note the assumptions that will affect the turbine's real power curve: electrical and mechanical efficiencies were

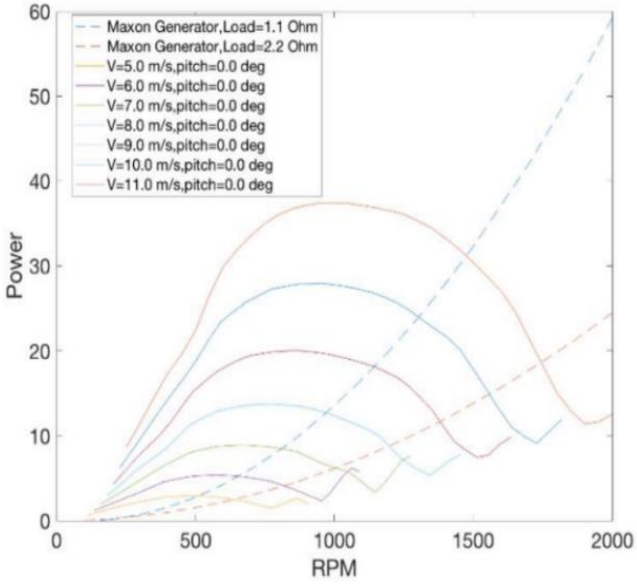

Figure 5. Blade power curve at 5-11 m/s.

approximated. More information on the generator can be found in the Power System and Controls Sub-Team section of the report.

The performance of this base blade design was evaluated through tunnel testing during the 2018-2019 and 2019-2020 year. Shown in **Figure 6** is the generated power curve from this testing data, where the circles are the measured power at each windspeed. The final design displays a cut-in at well below 5 m/s and a balanced power curve. The ideal cut-in angle of 4° were chosen because it allowed the turbine to generate enough power to pitch to a more efficient power angle between 7 m/s winds. At that point, the pitch control allows the blades to change the angle of attack to 8.5 degree, leading to a rated power of 27 W. During last year's competition, this blade design performed as expected, supporting this year's decision to keep the same base design.

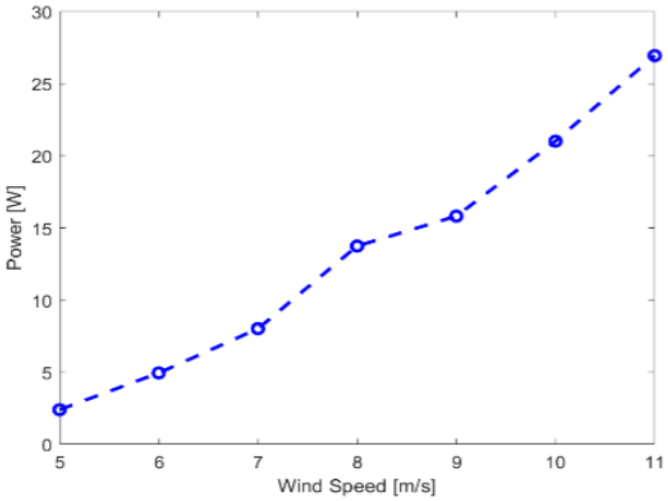

Figure 6. Experimental data using 2.2-ohm resistive load. At 7 m/s the pitch was changed for maximum power production.

An important addition of this year's competition was the addition of measuring the runaway speed for the cut-out task. By using a MATLAB code written to calculate the coefficient of power, a Cp vs. Lambda curve at 25 m/s was made. The tip speed ratio at the intersection of the x-axis is used to calculate the angular velocity of the turbine spinning at the runaway speed. Looking at **Figure 7**, the tip speed ratio is roughly 4.4 at the intersection point with the x-axis, translating to 4300 rpm for our turbine. This is an important value for the Electrical and Mechanical Sub-Team to use as a benchmark to design a structurally and electrically safe system.

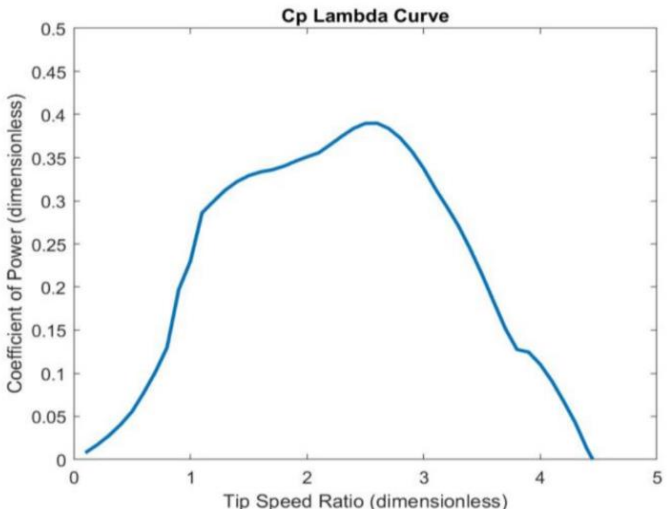

Figure 7. Cp-Lambda Curve for 25 m/s.

Winglet Design

The Aerodynamic Sub-Team was inspired to design and incorporate winglets, an innovative yet common feature on commercial airplanes that could potentially improve the turbine's overall performance. Winglets are small extensions to the end of a wing or blade that improve its aerodynamic performance. When attached to an airplane, winglets improve the lift to drag ratio of the wing, aiding in take-off and landing operations in addition to lowering fuel consumption. On horizontal axis wind turbines, winglets can increase power production. Although winglets on horizontal axis wind turbines have been studied previously, these studies can be difficult to compare due to differences in methods, scaling, and design criteria. Consequently, two different prototypes were developed to emphasize design elements from successful studies and were scheduled to be tested in March.

To better visualize how these winglets fit onto the blade, the following 3D model has been created in SolidWorks. **Figure 8** below shows how the first prototype winglet looks when attached to the blade.

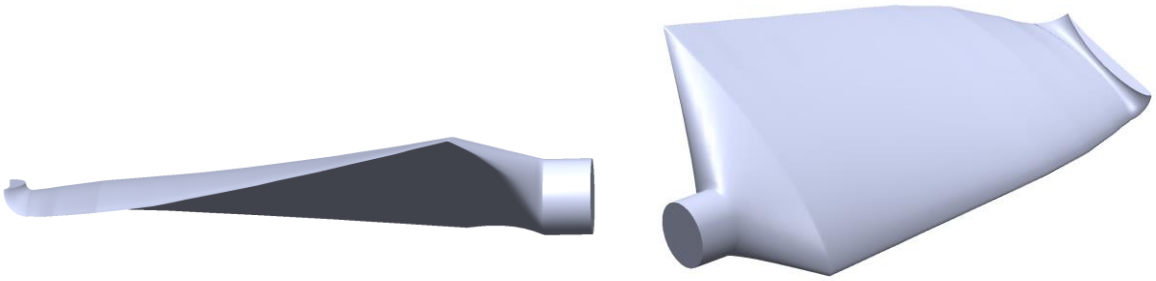

Figure 8. First winglet prototype attached to the blade design from last year (see Figure 4), created in SolidWorks.

To ensure comparability, all designs abided by a series of constraints. First, the winglets were designed to fit within the 45 cm cube around the turbine when attached to a single set of blades such that no set of winglets would result in a larger rotor diameter. Additionally, all winglets were designed to extend downwind from the blade at an angle normal to the blade tip. The downwind winglet was proven effective in an aerodynamic study using Computational Fluid Dynamics (CFD) by Jeppe Johansen and Niels Sørensen at the Risø National Laboratory of Denmark in 2006.[6] Of the six blade tips examined during the study, the small, downwind winglet improved power production and thrust the most. Johansen and Sørensen also emphasized the importance of an experimental -2° twist along the winglet .[6] Eleven years later, Thomas Hansen and Franz Mühle at the Norwegian University of Science and Technology used a series of models to obtain an optimal winglet design for a turbine prototype .[7] This approach also resulted in a minor negative twist along the winglet.

The two winglet prototypes contain similar elements inspired by published reports, but each prototype has a different design emphasis. The first winglet prototype was designed to be small and minimalistic. This design was inspired by Johansen and Sørensen's downwind winglet. These small winglets minimize the added weight to the tip of the blade while incorporating theoretically beneficial design elements. To assist with the design of the pitch control, the minimization of the weight should prevent additional difficulties in pitching the blades in or out of the wind. Additionally, using a smaller winglet design will of the inertial forces acting on the spars connecting the blades to the hub when compared to a larger winglet. The winglet extends past the tip of the turbine blade with a height equivalent to 1% of the rotor diameter. The tip is approximately 20% smaller than the root of the winglet. This small taper was created while keeping the leading edge at the same position relative to the tip of the blade to mimic the tip of the blade. The first prototype is shown to the left in **Figure 9**, looking from the last airfoil of the blade with the leading edge on the right.

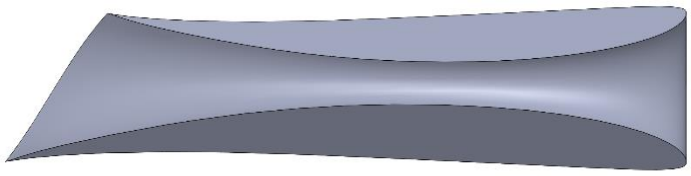

Figure 9. First -winglet prototype created in SolidWorks. It is oriented with the root, where the winglet connects to the blade, facing forward.

The second winglet prototype (**Figure 10**) featured a more prominent design, done to mimic the optimal winglet design as created by Hansen and Mühle. The winglet extends past the tip of the turbine

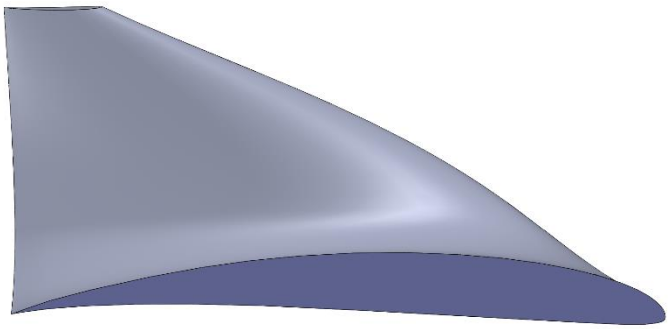

Figure 10. Second winglet prototype as designed in MATLAB. It is oriented with the root, where the winglet connects to the blade, facing forward.

blade with a height of approximately 5% of the rotor diameter-five times the height of the first prototype. The tip of the winglet is 60% smaller than the root of the winglet, creating a significant taper throughout the winglet. Unlike the first design, this winglet tapers with respect to the center chord of each airfoil. Finally, the design also features a small degree of twist (-2°) from the root to tip of the winglet.

A testing plan was created to compare the two winglet designs. Prior to testing, the winglets would be glued to the tip of the blade. The wind tunnel would operate at each integer wind speed from 3 to 11 m/s. At each windspeed, the angle of attack is varied from 0 to 15 degrees at a resolution of 0.1 degrees to find the maximum power produced at each windspeed. Once each winglet is tested with this method, the performance of each winglet design can be compared to that of the blade without winglets. The design with the highest expected points at competition would be selected.

Blade Manufacturing

When it comes to the blade manufacturing, some of the main factors initially considered were the quality, consistency, and mechanical properties of the blade. It is important for the sets of blades to be uniform in shape and weight, while also taking on the complex airfoil shapes with little to no variation or defects. For this reason, initial blade prototypes were created via 3D printing. 3D printing allowed for rapid prototyping, which meant that multiple iterations of different airfoil designs could be produced and tested. The filament used (ABS) also proved to have shear and tensile strengths necessary to withstand the forces exerted on the blades during testing. In addition, the quality of the printer used offered a favorable resolution, meaning the surfaces of the blades were smooth and uniform. This uniformity in production also meant small variations in weight between three blades in each set.

Although 3D printed prototypes were mostly successful, there were still a few concerns that arose during manufacturing. Sporadic defects between printing layers were a cause for concern from a mechanical behaviors standpoint, while the overall heavy weight of blade iterations was also a concern. For these reasons, an alternative manufacturing method was sought after for the final set of blades. The most viable option was decided to be a 2-part, expanding alumina polymer. This polymer matrix has favorable mechanical properties when compared to ABS, while also offering a significant reduction in blade weight. Additionally, the surface finish of these blades would be smoother than the extruded ABS iterations, allowing for more consistent aerodynamic performance. To produce these blades, a negative mold must be machined with the finalized airfoil design and coated in order for the composite foam not to stick upon pouring. An additional measure for uniform blades with minimal defects is the inclusion of outgassing holes around the perimeter of the mold. These will ensure proper expansion through the mold geometries, as well as prevent air pockets within the blades themselves.

The manufacturing plan was to prototype iterations of differing airfoil designs using ABS, then once a final design was settled upon, machine a negative mold in order to create a set of lightweight, foam polymer blades.

Mechanical System

Introduction

The Mechanical Sub-Team is responsible for all mechanical components of the turbine, from the tower to the blades. In the past, this team has been split and worked on projects independently, but this year all mechanical design happened simultaneously. With the addition of milestones and the new competition tasks, the mechanical team set to designing as many robust systems possible. Some projects were taken from past years and improved for safety and efficiency, while others were designed from the ground up. This combination of projects provided students the opportunity to see how design can be handled in industry, either to improve what exists or starting from scratch. The following section details the process and design decisions involved in creating functional pitch control, mechanical braking, and passive yaw systems.

Drive System

The mechanical team wanted to push the efficiency of our turbine as much as possible this year, so a differential drive shaft system was considered. An advantageous gear ratio would potentially increase the amount of power the team could harvest from certain wind speeds, as is the case with many full-sized wind turbines. The team considered three design options: a fixed gear ratio that would keep the torque and speed ratios on either side of the drive shaft constant, a variable gear ratio that we would be able to control and optimize through various wind speeds, or the single speed drive shaft. Although a variable gear ratio would be useful (as the optimal ratio for low wind speeds is not the same as high wind speeds), a variable design would require an additional motor and control system. The team decided that this would not be feasible considering the additional strain of a third motor as mechanical brake and pitch control both required power.

As the team moved forward on the design of the fixed gear ratio, computations for the ideal gear ratio were performed. Using data gathered from last year's testing sessions, the cut-in torque can be determined from the generator torque speed characteristic and power data. The average cut-in torque was found to be roughly 0.0615 N-m. By supposing a 2:1 gear ratio in the drive shaft, the torque needed to cut-in would increase to 0.123 N-m. The relationship between the torque and wind speed data was then used to approximate the cut in speed of the hypothetical system to be 9.5-10.5 m/s. Increasing the cut-in speed would decrease the amount of points the team could be awarded in the Power Curve Performance task, whether the power output was doubled or not. As creating smaller gear ratios and two-stage systems would require more space in the body of the turbine and still increase the cut-in speed it was decided that this year's turbine design would not include a differential drive shaft.

Pitch Control

Our pitch control system consisted of a very similar design to last year's turbine, with minor changes to utilize space more effectively. **Figure 11** below shows the pitching system with labeled parts. In general, the system developed last year converts translational motion within the drivetrain into rotational motion of the blades. The pitching system operates by mounting a brass pinion gear **(a)** on each blade and moving the blades together with three separate racks **(b)** all mounted to a singular plate **(c)**. The blades are pitched by moving the plate forward and backward relative to the fixed position of the blade spars, rotating the blades by an amount corresponding to the plate's displacement from its original position. The drive shaft **(d)** is mounted inside an outer aluminum sleeve **(e)** with the plate **(c)** mounted on one end of the sleeve. The sleeve is then mounted within two radial bearings rotating with the drive shaft. These bearings are secured in two aluminum housings **(g)** and mounted on lead screws **(h)** which were positioned on either side of the housing's central bearing. As the lead screws rotate, the housings are either pushed or pulled, which transfers the motion to the racks inside the hub **(f)**. This rotation is accomplished with a single stepper motor **(i)**. The stepper motor and each lead screw have a timing belt pulley fastened to their ends, and the timing belt is routed between the pulleys **(j)** to transfer the rotational motion of the stepper motor to each lead screw accurately. Additionally, the bearing housings are fastened together by an aluminum bar on their undersides, and a linear rail **(k)** was installed on the bottom of this bar. Two linear carriages **(l)** were

mounted to the baseplate of the turbine and the linear rail was inserted into these carriages, allowing the vertical forces and moments to be primarily carried through the linear carriage as opposed to the lead screws.

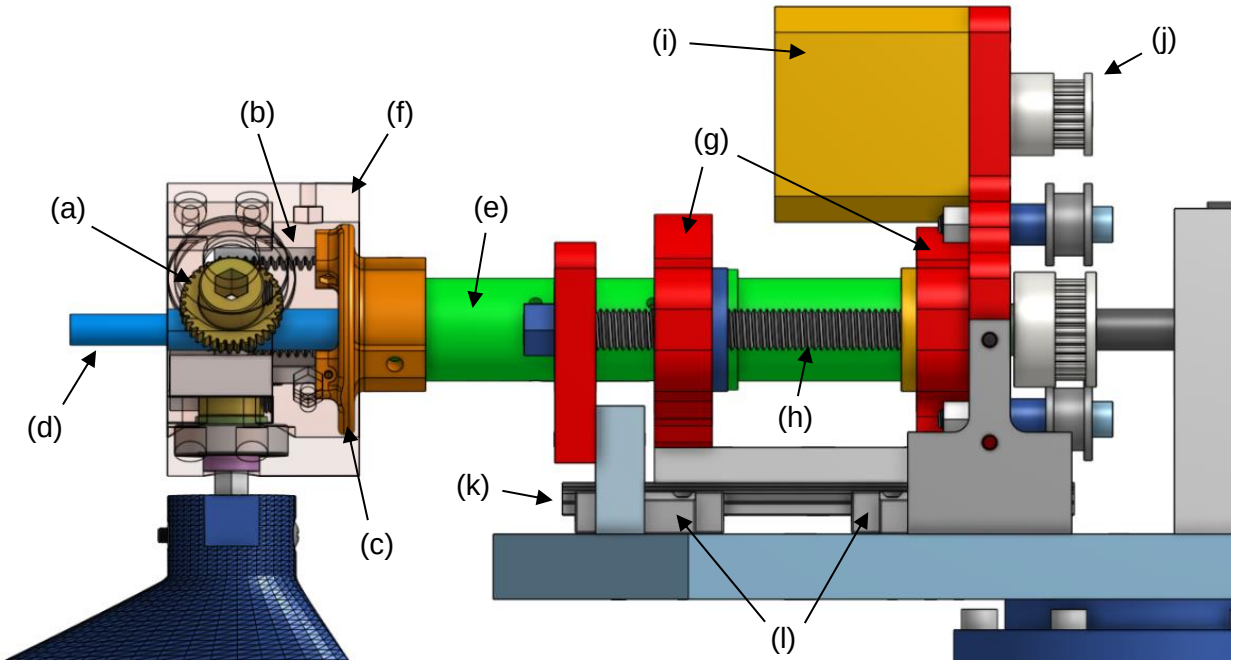

Figure 11. Pitch control assembly with labeled parts.

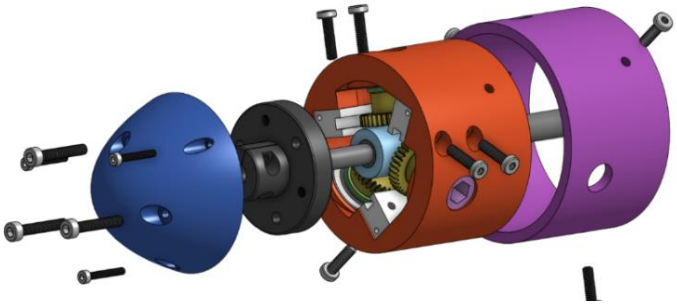

Figure 12. Exploded view of the aluminum (purple) reinforced hub.

After the team concluded that the destructive failures the hub experienced the previous year were caused by high stress concentration in its geometry, one of this year's objectives was to fortify the mechanical system. In parallel with the purpose of the rotor strength mid-year milestone, the team chose to focus on designing a stronger hub. With a stronger hub, the turbine would have the potential to withstand the high speeds of the runaway condition. However, redesigning the hub brought numerous challenges, as we had to consider the assembly process, machinability, and complex geometries of the hub. Our team considered various changes to the parts inside the hub as well as ideas to reinforce the exterior. Our first design iteration, shown in **Figure 12**, involved redesigning the outer geometry of the hub to be circular and then screwing a ⅛ in. cylindrical aluminum sleeve over the exterior of the hub to transfer stresses in the plastic hub core to the metal sleeve and prevent fracturing during testing.

To ensure the redesigned hub would safely operate at the 4300 RPM for the rotor strength test, the team performed finite element analysis. Because the interactions between the hub core and the aluminum sleeve are very complex, an analysis was performed on the sleeve alone to determine if the ⅛ in. wall thickness would be enough to prevent failure at high speeds. The simulation was run using the rotational speeds we expect in the rotor strength test and a blade mass of the heavy 3D printed blades. **Figure 13** shows the analysis with respect to stresses, where concentrated stresses can be observed at the holes cut for the blade spars and the bolts connecting the inner and outer hub sections. The maximum stress observed is 31.4 MPa while the yield strength of aluminum is roughly 227 MPa corresponding to a 7.2 factor of safety in yielding. This is a considerable improvement on last year's design.

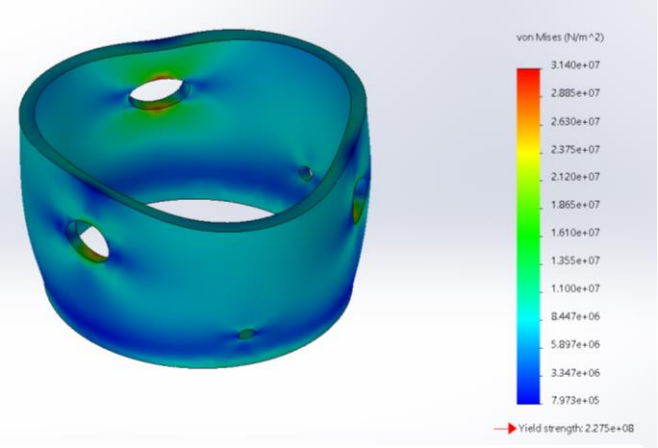

Figure 13. Stress based finite element analysis on aluminum reinforcement sleeve shows 7.2 factor of safety.

This reinforcement required an increase to the overall size of the hub. With the size constraint on the turbine diameter, this meant slightly shortening the blades. As the swept area is directly proportional to the power we can generate, the change did decrease our potential power, but the increased safety was deemed worth the loss. This updated version of the hub was tested during the rotor strength milestone and performed well. At 2500 RPM, a blade dislodged from the hub but the hub itself remained completely intact with no signs of fatigue or cracking. After further analysis, the team concluded that the set screw of the pinion gear was not fixed deep enough into the spar of the blade, and the vibrations at high speeds caused the screw to come loose, which led to failure. To address this issue, we updated the design of the spar holes to make them more pronounced and added Loctite to the set screw to prevent vibrations from loosening it. The team also decided to switch the pinion gears to ones with built-in set screws to ease the machining process and ensure correct tolerancing.

Following the rotor strength test the team decided to work on further improvements to the hub. The existing hub required the 3D printed nose cone to transfer motion from the hub itself to the drive shaft. The blades generate lift, causing the hub to turn. The hub was attached to the nose cone which was connected to a flanged shaft collar fixed to the drive shaft. To connect the shaft collar directly to the hub involved a redesign of the rack blocks (which anchor the nose cone) and the hub itself. First, the ⅛" aluminum sleeve would be replaced with a ¼" sleeve so an aluminum cap can be placed on the end of the hub and screw directly into the outer sleeve. That way, the flanged shaft collar can screw into the hub cap, making the nose cone purely aerodynamic. Next, to fix the issues discovered in the rotor strength test, the team decided to change from ¼" hex spars to regular ¼" circular spars. This format allows for gears that are sized directly for ¼" spars with machined set screws with better tolerance than the gears the students are able to manufacture. The more precise hardware, in conjunction with the Loctite mentioned earlier, will prevent blades from slipping loose of the hub. This redesign, shown in **Figure 14**, also allows for the elimination of the stress concentration in the inner hub that caused failure in the past. The rack blocks that act as a guide for the gear racks can be

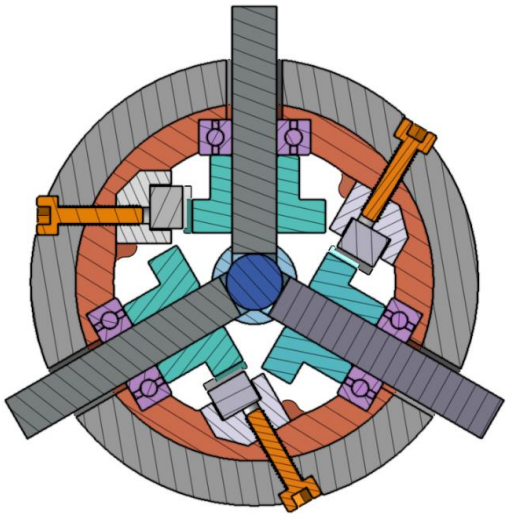

Figure 14. Section view of the latest hub iteration with cylindrical ¼" spars.

chamfered because the nose cone no longer needs to attach to them. The chamfer eliminates the sharp 90° corner that caused cracking at high wind speeds in past hub iterations.

Considerable testing would have gone into validating the latest hub iteration, however the COVID-19 pandemic caused physical work on the turbine to end. The team had multiple testing procedure prepared to ensure the redesigned hub worked well. Between testing periods, the dynamometer fixture would be used to test the precision and repeatability of pitching and calibrate the control system. Once wind tunnel time could be secured, the hub would be run through the competition tasks. Additionally, a second rotor strength test would be performed to identify the next area of weakness where improvement could be made.

Mechanical Brake

At the 2018-2019 competition, our team did not earn any points for the safety task. Pitch control and generator braking were used in conjunction to slow the turbine, but those systems alone were not enough to accomplish the task. This year, the addition of the cut-out task pushed our decision to add a mechanical brake system to slow the turbine when needed. The team decided to implement a disc brake system similar to what is used on bicycles. The disc brake is relatively simple to manufacture while providing extremely quick stopping power.

Figure 15 to the right shows the brake assembly with labeled parts. The mechanical brake operates by clamping a disc **(a)** fixed to the drive shaft with two brake pads. One pad is stationary **(b)**, located very close to the disc while the other moves **(c)**, determining the clamping force. The moving brake pad is fixed to a flange nut carriage **(d)** that travels linearly when the lead screw is rotated by a stepper motor **(e)** located below the baseplate. Similar to the pitch control system, a timing belt pulley system **(f)** ties the stepper motor to the lead screw with an adjustable idler pulley **(g)** used to tension the belt. The location of the motor is critical in keeping the turbine within size constraints. The hub, pitch control, generator, and disc all take space along the drive axis while the space below the baseplate was not being used. Additionally, the disc was made as large as possible by removing material in the baseplate where the disc needs to rotate. The brake pads are mounted using two L-brackets **(h)** on either side of the disc to allow space in the baseplate for the disc. A larger disc radius requires less force to stop as the applied friction results in a larger moment the farther from the axis it is applied. Finally, a shaft support **(i)** is mounted at the end of the drive shaft for increased stability with the large applied moment at the brake disc.

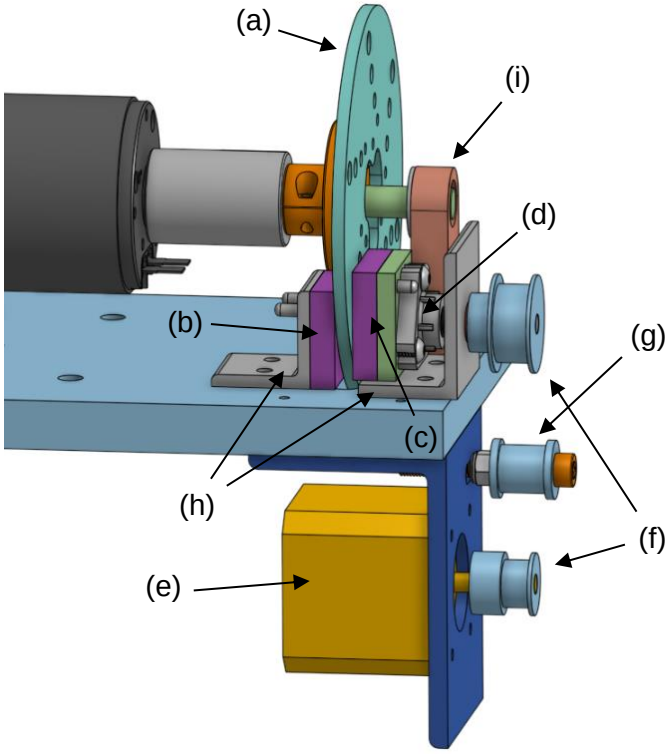

Figure 15. Mechanical brake assembly with labeled parts.

The team had to ensure that the stepper motor could provide sufficient torque to stop the turbine. The first calculation was finding the inertia of a single blade and multiplying it by three to achieve the inertia of the entire system. This rough computation ignores the relatively small contribution of the generator and bearing friction compared to the mass of blades. In addition, this inertia was calculated using the mass of the 3D printed blades, which would be significantly heavier than the final foam blades, thus resulting in a conservative calculation. Then, we found the maximum angular acceleration based on runaway speed, calculated at 4300 RPM. Using this speed ensures even if we were to completely lose control and approach runaway, the mechanical brake would be able to handle it. The torque required to stop

the turbine at runaway speed in ten seconds was determined to be 0.177 N*m. The stepper motor we planned to use can deliver 0.59 N*m of torque, more than capable of providing the power we need, even ignoring mechanical advantage built in from the lead screw.

Although the team was unable to test the mechanical brake, the plan was to put it through testing in the wind tunnel to ensure success of the cut-out task at competition. In order to test between tunnel testing periods, the dynamometer fixture designed earlier in the year could have been used to test the effectiveness of the brake. The dynamometer runs in a constant current setting, so when the brake is applied the motor will continue to try and drive the system to the set RPM, simulating the constant torque the wind would apply to the blades.

Yaw System

The yaw portion of our turbine was another focus for our team this year. We began with generating concepts including active and passive yaw. The active yaw had the potential to be more responsive than the single tail design implemented last year which had difficulty maintaining a perpendicular facing at all wind speeds. However, after further development of the idea the team began to see many drawbacks with active yaw. We would need to add a third motor to the electrical system with the possibility that the motor would always require power. If the system was designed with the proper gearing to prevent that, the response might not be fast enough to maintain proper direction during the durability task. Furthermore, the system of gears needed to prevent back driving the motor could not be feasibly mounted within the 15-centimeter diameter constraint for the tower. For these reasons, our team decided to proceed with a passive yaw design.

The biggest problem with a passive yaw design was space. With the addition of the mechanical brake to the drive system, there was very little space behind the turbine for a single tail. Therefore, we investigated the use of non-traditional tails. The team considered two-panel tails at various angles, a honeycomb pattern, and curved tails. The two-panel design proved the simplest to implement, but we were not sure what angle or tail size would be the most efficient for our turbine. When considering the size of the tails, we found research indicating that the tail surface area should be 20% of the swept area of the blades. The information related to large scale aerodynamic applications which do not scale accurately to our turbine. To determine the ideal tail size, we chose three tails corresponding to 10%, 15% and 20% of the swept area of 1512 cm^2.

To allow for the tail angle to be adjusted, we mounted a 12” aluminum L-extrusion to the baseplate and attached two hinges at the vertical ends to the tail panel. To lock the tail at the angle of our choosing, a slot was cut in the horizontal plane of the mount. Then, another hinge was attached to the tail panel approximately two inches away from the first hinge, which was connected via a small L-bracket. This hinge was attached to an arm whose end could be tightened in place using bolt in the slot. The resulting hinged two panel tail was designed to be fixed at any angle between ±30° of perpendicular. This assembly is shown in **Figure 16**.

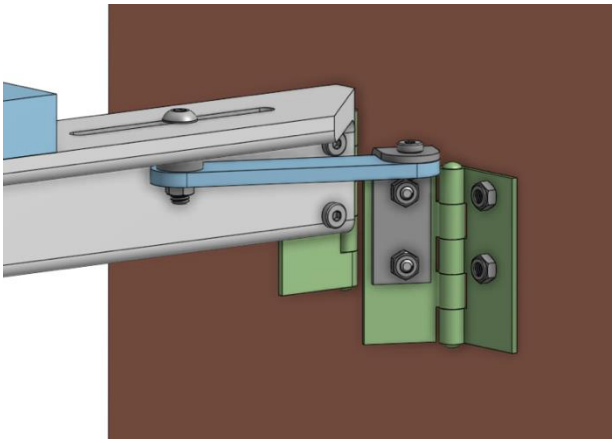

Figure 16. Adjustable yaw assembly.

During an early testing session in the wind tunnel, we performed testing at 10° increments to qualitatively determine which tail angle faced the wind most directly and responded quickest to changes in wind direction (by rotating the baseplate and allowing the tail to re-orient). We repeated testing for each size panel fabricated and found that the largest panel was the only one that was relatively responsive. As a result, we planned to fabricate and test another set of tails with the 20% swept area as the smallest size.

Power Systems and Controls

Introduction

The objective of the electrical and control design of the turbine is to maximize power output to the load while maintaining a safe operating point for all conditions. The key components of the design include: generator selection, load design, software and control system development for microcontroller board, sensing circuits, actuation of certain mechanical systems, and a maximum power point tracking (MPPT) system. A mathematical model was created in MATLAB to simulate the turbine's steady-state behavior. A full system layout is shown in **Figure 17**. Red lines in the diagram represent power flow and green lines show signal flow.

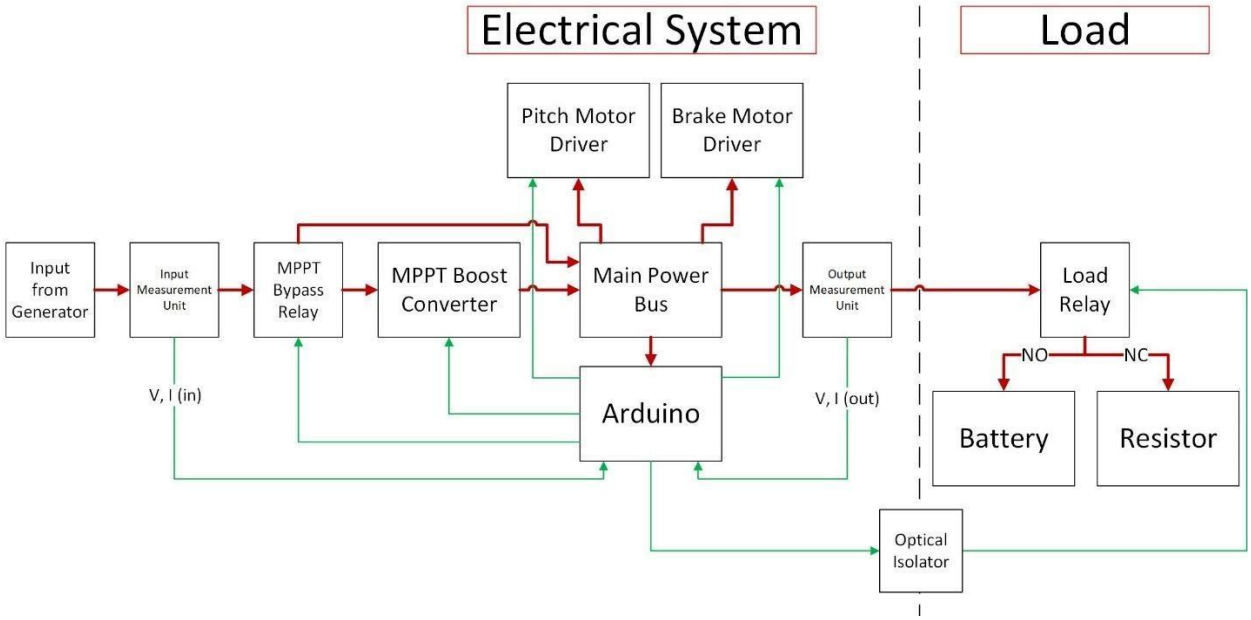

Figure 17. Full electrical system and load layout.

Generator Selection and Analysis

To convert the mechanical energy of the rotating shaft to electrical energy, the team selected the Maxon RE 50, shown in **Figure 18**, as the turbine's generator. The Maxon RE 50 is a permanent magnet (brushed) DC (PMDC) motor. While DC generators are typically avoided on utility scale wind turbines due to their size and both losses and increased maintenance costs due to the brushed commutator, for this application these issues are diminished. The operating life of this application is short enough that wear on the brushed commutator is not a concern. Additionally, since the desired power output is DC, the brushed generator avoids the need for rectification that AC motors have. Diode-bridge rectifiers are a non-negligible source of loss and sizing the smoothing capacitor becomes incredibly important. Inevitably, the output will be left with some voltage ripple. The output of the PMDC generator, on the other hand, is smooth DC, and any fluctuation is a result of variations in the rotation of the turbine. Qualitatively speaking, Maxon motors spin the smoothest compared to

Figure 18. Maxon RE 50 Motor.

other motors (AC and DC) tested by the team, which means low frictional losses in the internal bearings and brushed commutator.

In the previous year's design, a major factor in the generator selection process was the current characteristic as a high current was needed to adequately charge the ultracapacitor used to regulate a constant 5 V in highly variable conditions. This led to the team selecting this generator, which was successful in charging the ultracapacitor. However, since ultracapacitor charging is no longer a necessary function of the turbine, the high current characteristic of the generator detracts from the overall system performance. Based on the blade power curves in **Figure 5**, the blades can output a maximum of 38 W at roughly 1000 rpm at rated wind speed. Using the speed constant of the selected version of the Maxon RE 50 of 248 rpm/V, the ideal rated voltage and current is 4.03 V and 9.42 A, which is a resistance of 0.43 Ω. The wires connecting the generator to the system alone account for 0.253 Ω (10 ft of 14 AWG wire at 0.0253 Ω/ft) and the internal resistance of the generator adds 0.103 Ω. If the blades were to produce their rated power, over half would be lost in I^2R losses before it could be delivered to the load. This shows that the generator and the blades are mismatched. An MPPT system was added to help account for this mismatch, but switching to a generator with a higher speed constant would mean at the same rotational speed, the generator would produce a higher voltage, which would increase the ideal load resistance to match the blade curves and therefore decrease power loss in the wires, allowing for a better match between generator and blades.

Load Design

The team wanted to design a load that would be able to use the power generated by the turbine during normal operation, while also supplying the turbine with power in emergency situations. Being able to draw energy from the load while the turbine is stopped for safety reasons was a priority, as most reliable stopping mechanisms require energy to actuate. Another design requirement was that the load must be able to accept energy at cut-in and low wind speeds. The team started with two main alternatives for energy storage: an empty ultracapacitor that would be charged as the turbine generated power, then discharged as the turbine needed energy; or a resistor and a pre-charged battery in parallel with a switch to select one of them.

Both of these options met the two criteria: they can draw or supply energy depending on need and can accept initial energy at any voltage. However, the resistor and back-up battery were chosen for two main reasons. First, because the current in a capacitor $I_C = C\,dV/dt$, the effective resistance of a capacitor $R_C = V_C/I_C$ is dynamic as the capacitor charges, making both optimization of the load and control of output power more difficult. The resistor can be selected to match the turbine and remains static throughout the operating modes of the turbine. Second, the only energy available to the system during shutdown would be the energy generated by the turbine. During an extended downtime, this could mean the possibility of losing power and either inadvertently restarting or losing the ability to restart. The battery can be sized to provide power for the worst-case scenario.

The turbine's load consists of a resistive load for all power generating tasks (Cut-in, Power Curve, Control of Rated Speed/Power, and Durability), a back-up battery supply for turbine shutdown tasks (Safety, Cut-out and Parked High Wind), and a latching relay to switch between them. The signal to switch the relay comes from the Arduino in the main system, is optically isolated, then used as the input to a current amplifier capable of powering the relay's coils. The latching, or bistable, relay is shown in **Figure 19**. and is a double-pole single-throw (DPST) relay that has two stable positions and only requires power to switch positions. In the load, the two poles of the relay are tied together, making it behave like a single-pole double throw (SPDT) relay.

Figure 19. Latching relay.

Because of the MPPT system in place, the resistance value could be chosen without considering the blade / generator interactions. The DC-DC boost converter with an adjustable output allows the control system of the turbine to transform the static load resistance into a dynamic system input resistance. Considering the power available in the wind and the predicted turbine output at all wind speeds, the

resistance value was chosen to balance the voltage level of the system. If the resistance value is too low, the voltage generated at low wind speeds is low as well, which makes biasing electronics more difficult. If the value is too high, the system could exceed the 48 V maximum at higher wind speeds. A value of 20 Ω was chosen because throughout the power curve the voltage in the system is high enough to bias the electronics (Arduino, converters for stepper motors) and I^2R losses in the wires leading to the load are reduced compared to a smaller resistance value. Additionally, a 20 Ω load requires 115.2 W to exceed the 48 V maximum. At roughly 4 times rated power, another component of the turbine would certainly fail before the turbine would experience an overvoltage.

Figure 20. Selected lead acid battery.

The battery was chosen such that the nominal voltage is appropriate for the electronics it must power, and the desired capacity would allow the battery to last throughout the entire turbine prototyping and testing phase. A 12 V, 7.2 Ah sealed lead acid battery, shown in **Figure 20**. was selected to be the back-up power supply. 12 V is within the accepted input range for most electronics or can be easily adjusted using commercial DC-DC converters. The capacity is sufficient to maintain a minimum of 6 hours' worth of supply with worst-case loads. Strategic minimization of load (not using the pitch system during shutdown) can increase this time even further. A calculation of the minimum duration of the storage element is shown below. The physical size of the battery is also manageable.

The possible loads on the battery are: (i) Arduino Uno with all output pins high: ≤ 2 W (ii) Stepper motor for pitch control: ≤ 6 W (iii) Stepper motor for mechanical brake: ≤ 6 W (iv) Two Relays: ≤ 0.4 W. This results in a total load of 14.4 W. The rated battery capacity is 86.4 Wh, therefore the battery can supply the worst-case loads for 6 hours. At 30 minutes per testing run, the battery can be expected to last for no shorter than 12 testing runs, although realistically will last much longer since the battery is only used when the turbine is shut down.

Turbine Control

An Arduino Uno microcontroller board was selected to function as the turbine's center of control. It continuously polls measurement and sensing circuits, makes decisions based on operating conditions, and sends actuation signals to stepper motors and relays accordingly. Its decision making is governed by a finite state machine (FSM) structure designed around the competition's tasks.

Measurement and Sensing

A circuit was designed to allow the Arduino to measure voltage and current at both the input and output of the system. **Figure 21**. shows a printed circuit board (PCB) implementation of the measurement circuit. Measuring both the input and the output allows for better data on system performance, especially efficiency ($\eta = P_{Out} / P_{In}$). The turbine's RPM can be estimated by multiplying the input voltage by the speed constant of the generator. The circuit consists of an integrated circuit (IC) hall-effect sensor in series with the current being measured and a resistor voltage divider in parallel. The IC outputs a voltage proportional to the sensed current that the Arduino measures on an analog input pin and converts to a current. The voltage divider scales the measured voltage to a maximum of 5 V based on the Arduino's limit. The resistor values are selected based on the circuit's location and expected voltage range (determined experimentally with added margin), such that near the upper bound of the voltage range, 5 V, is dropped across the bottom resistor. A rolling average of measured values is kept, reducing noise and minimize effects of misread measurements.

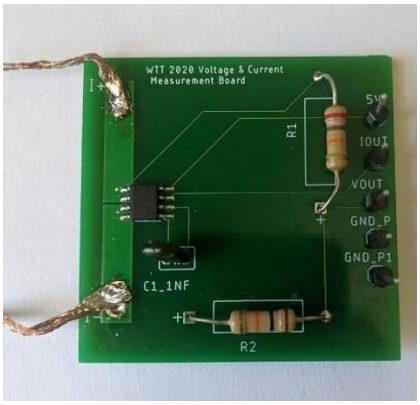

Figure 21. Measurement circuit PCB.

The Arduino also monitors the conditions for Safety task. The normally closed safety switch is connected between the 5 V pin on the Arduino and a digital input pin, with a 2.2 kΩ pull-down resistor to ground. The digital pin then reads high during normal operation, as it is directly connected to the 5 V pin. When the switch is open, the pin is pulled to ground by the resistor, meaning the pin will read low when the E-stop button is pressed. This design ensures that a maximum of 2.3 mA flows through the E-stop circuitry. A load disconnect is detected by the load output measurement circuit reading a non-zero voltage, but a near-zero current, which implies an open circuit at the load.

Finite State Machine and Task Operations

The finite state machine running on the Arduino is shown in **Figure 22**. The specific operations of each state and the conditions necessary to change states are described in **Table 1**. The Arduino controls the various turbine sub-systems to maximize power between 5 m/s and 11 m/s, maintain rated power above 11 m/s, and stop the turbine when necessary. During Durability Task, when the only goal is to produce power, there are two main failures to avoid. The first is the possibility of the turbine stalling, so the blades are positioned in a pitch angle that performs well at low wind speeds. The second is to prevent the main DC-DC converter from failing, so the output is set to a value that the turbine is capable of matching at all wind speeds.

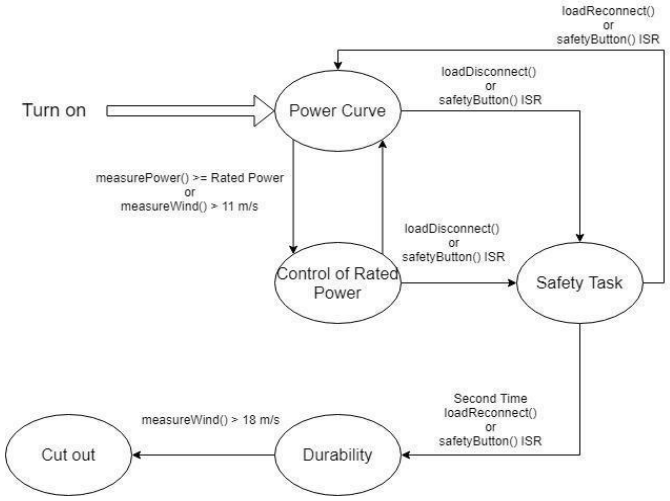

Figure 22. Finite state machine diagram.

Table 1. Description of FSM state functions and state change conditions.

State	Description and Functions of State	State Change Conditions
Power Curve	• Assumed to be the turn-on state of the turbine • Maximizes power delivered to the load by ▪ Positioning blades in optimal pitch angle ▪ Running MPPT algorithm	• E-stop button pressed or load disconnected, go to safety task • Output power > rated power, go to control of rated state
Control Rated	• Set MPPT converter output to rated • Run PID controller to maintain rated power by pitching blades • Rated power is pre-determined through testing	• E-stop button pressed or load disconnected, go to safety task • Output power drops significantly below rated, back to power curve
Safety	• Switch load relay to battery • Switch generator relay to ground • Apply mechanical brake	• Load is reconnected or safety button is un-pressed, depending on initiation method ▪ First trial, go to power curve ▪ Second trial, durability

Durability	• Establish desired conditions, then wait ▪ Blades in low-efficiency angle ▪ Set MPPT converter to achievable output	• Wind speed rises above 18 m/s
Cut-out	• Switch load relay to battery • Switch generator relay to ground • Apply mechanical brake	• Turbine requires manual reset after parked high wind condition

Pitch Control PID Controller

As the wind speed increases above rated wind speed, rated power is maintained at the load by holding the adjustable DC-DC converter output constant at the turbine's rated voltage. With no other systems in place, at a higher wind speed, the turbine will accelerate and torque will decrease while power remains the same. An additional control system is required to maintain the rated rotor speed at high wind speeds. The team designed a feedback controller to control rated power above 11 m/s using the pitch control system. The controller compares the measured power to the rated power at 11 m/s and adjusts the pitch using the PID controller algorithm shown in equation {1} where θ is the pitch, e is the difference between power and rated power, and K_P, K_D, and K_I are gain constants.

$$\theta(t) = Kp * e(t) + Kd * \frac{de(t)}{dt} + Ki * \int_0^\tau e(t)\, d\tau \quad \{1\}$$

To easily choose gains analytically, the team used a simple model that assumes a constant generator load and ignores the drive shaft. The model is shown in equations {2} through {3}, where ω is the angular velocity of the turbine, J is the rotational inertia, T_a is the torque produced by the blades, T_g is the torque produced by the generator, V is wind speed, θ is the pitch angle, η is the efficiency from electrical and mechanical losses, and P is the power output of the generator.

$$\frac{d\omega}{dt} = \frac{1}{J} * \big(Ta(\omega, V, \theta) * \eta - Tg(\omega)\big) = f(\omega, V, \theta) \quad \{2\}$$

$$P = h(\omega) \quad \{3\}$$

Linearizing this model at a wind speed, pitch angle, and rotational speed design point yields equations {4} and {5} with constants $a = \frac{\delta f}{\delta \omega}$, $b = \frac{\delta f}{\delta \theta}$, and $c = \frac{\delta h}{\delta \omega}$.

$$\dot{\omega} = a * \omega + b * \theta \quad \{4\}$$

$$P = c * \omega \quad \{5\}$$

Finally, a closed loop transfer function was derived by taking the Laplace transform of equations {1} through {5} that relates the power output of the turbine to the rated power output, shown in equation {6}. By choosing K_P, K_I, and K_D, the denominator of this transfer function can be tuned to achieve the desired response.

$$\frac{P}{P_{rated}} = H = \frac{cb(Ki + sKp + s^2 Kd)}{(cbKd+1)s^2 + (cbKp - a)s + cbKi} \quad \{6\}$$

The benefit of choosing a simple model is that it resembles a second order response equation {7}.

$$s^2 + 2\xi\omega s + \omega^2 \quad \{7\}$$

The damping ratio, ξ, and natural frequency, ω, can be defined by specifying a settling time of 10 seconds and a maximum overshoot of 1% which then inform the values of K_P, K_I, and K_D. These high-performance values were chosen to account for the expected decrease in performance from ignoring dynamics and to ensure that the turbine would settle at rated power well within the requirements of the competition.

Maximum Power Point Tracking

The interactions between the blades, the generator, and the electrical system ultimately determine the operating point of the wind turbine for a given set of conditions. The ω vs. P curves of the blades show that at each wind speed there is a maximum amount of power that they can extract from the wind and that it occurs at a single rotational speed. The goal of the MPPT system is to dynamically adjust the electrical load presented to the generator to deliver maximum power to the load resistor throughout the power curve task. This is done by implementing a DC-DC boost converter whose output setpoint can be adjusted by the

Arduino. The output setpoint along with the static resistance value determines the output power of the electrical system. The blades will naturally change their speed and torque as the converter output is adjusted. Using the DC transformer model of the converter, the load resistance can be reflected to the input of the converter to determine the load seen by the generator. For a boost converter, the input resistance will always be lower than the load resistance. Therefore, the load resistance can be selected independently from the generator and blade characteristics.

During wind tunnel testing, the team utilized a commercial-off-the-shelf DC-DC boost converter whose output was set using a trimming potentiometer to test operating principle. At each wind speed in the power curve, the converter was adjusted to find the maximum power the turbine was able to deliver to the load. By measuring input voltage and current throughout this process, the optimal input resistance was found throughout the power curve. These results are shown in **Figure 23**. and are plotted against a static 2.2 Ω, which was load resistance used for the previous year's turbine. This plot indicates the usefulness of a dynamic system to match the load to the blades, as the ideal resistance varies significantly throughout the power curve.

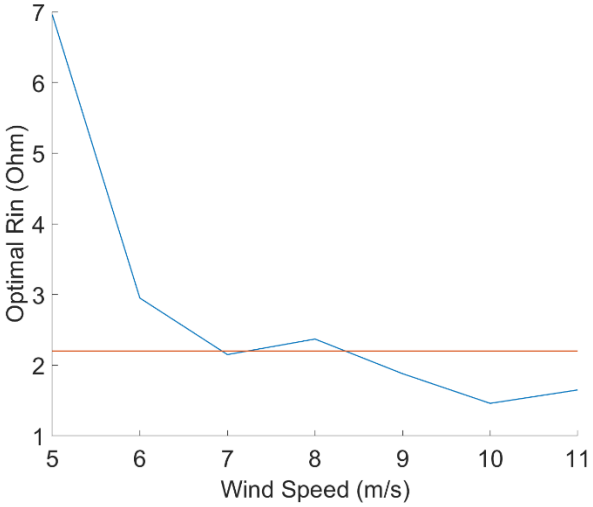

Figure 23. Optimal input resistance across power curve wind speeds.

MPPT Bypass Circuit

When the system is drawing power from the load, the DC-DC boost converter used in the MPPT system needs to be disconnected from the rest of the system so the power from the battery does not affect the power electronics. The generator terminals are also shorted together to begin the turbine shutdown process. Connecting a very small resistance to the generator increases the torque required to spin the turbine, which slows down the turbine's rotation and reduces the load on the mechanical brake. Both are accomplished using the same model of bistable DPST relay as is used in the load. The diagram in **Figure 24**. shows the normally connected (NC) pole and throw linking the output of the converter to the rest of the system and the normally open (NO) pole and throw between the positive and negative terminals of the generator. During braking operation, the NC connection opens, and the NO connection shorts.

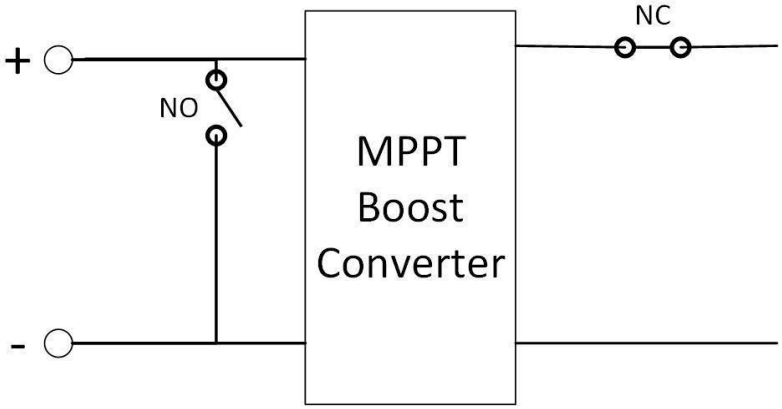

Figure 24. MPPT bypass circuit diagram.

Turbine Model

During the development of the MPPT system and the analysis of the generator selection, it was useful to create a mathematical model of the turbine in MATLAB that could be used to be determine the steady-state operating point at any conditions. A diagram overview of the model that includes the MPPT system is shown in **Figure 25**. A version of the model with only the resistive load was also created.

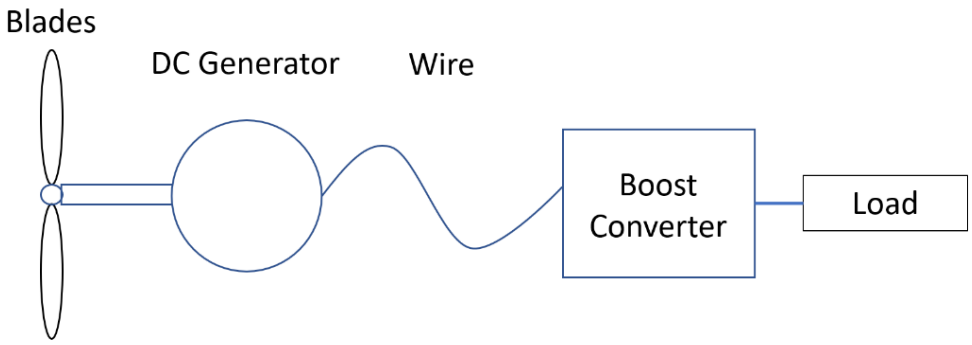

In the MPPT version, the inputs to the model are converter output voltage setpoint and wind speed.

Figure 25. Turbine model diagram overview.

An iterative minimization algorithm is used to find the operating point that minimizes the difference between mechanical power in the blades and electrical power in the generator, obeying conservation of energy. The power output of the generator is calculated using V^2 / R in the load, reflecting the resistance to the input of the boost converter using the DC transformer model, and calculating I^2R losses in the wire and internal resistance of the generator. The search variable for the minimization is the boost ratio of the converter, which is necessary for reflecting the load and calculating the input voltage to the converter. Based on the calculated voltage at the terminals of the generator and the speed constant, the rotational speed of the direct drive system is determined, which is used in the blade power calculation. The power output of the blades is calculated using a table of Cp-λ pairs provided by the Aerodynamics team and the power available in the wind at the given wind speed. This model allows the team to predict the maximum power the turbine can produce at each wind speed and turbine behavior at different converter output setpoints. Analyzing model results also suggested improvements that could be made to the turbine to better match the generator and blades.

Prior to the stoppage of physical work on the turbine, the entire circuit layout, as seen in **Figure 17.** had been completed. The measurement circuits had been designed, prototyped, and fully implemented on a PCB, seen in **Figure 17.** Several sub-circuits, including the MPPT bypass circuit and motor drivers had been designed and prototyped and the PCB layouts were in progress. The load circuit, primarily the optical isolation and switching mechanism, was being prototyped and debugged. Conceptual design and testing using commercial products had been done on the MPPT system and original design and algorithm development was beginning. The desire to continue work on this part of the design led to the creation of a computer model of the turbine that was used to experiment with algorithms, predict results, and validate the need for a dynamic tracking system. Had physical work continued, that effort likely would have been focused on the hardware and practical software components. Instead, a tool was created that immediately paid dividends by highlighting a weakness in the design that can be easily corrected. The circuit implementations that were completed in early 2020 as well as the software model created in the second half of the Spring 2020 semester will serve the team in the future as they continue to improve the reliability of the turbine and innovate where possible.

References

[1] Kulunk E, *Aerodynamics of Wind Turbines, Fundamental and Advanced Topics in Wind Power*, New Mexico Institute of Mining and Technology, 2011.

[2] Maheri A, Noroozi S, Toomer C, Vibbey J, *Damping the fluctuating behaviour and improving the convergence rate of the axial induction factor in the BEMT- based rotor aerodynamic codes*, University of the West of England, 2006.

[3] Ning S A, *A simple solution method for the blade element momentum equations with guaranteed convergence*, National Renewable Energy Laboratory.

[4] Shen W Z, Mikkelsen R, Sorensen J N, *Tip Loss Corrections for Wind Turbine Computations*, Department of Mechanical Engineering, Technical University of Denmark, 2005.

[5] Arora J S, *Introduction to Optimum Design*, 2017.

[6] Johansen, J., & Sørensen, N. N. (2006). Aerodynamic investigation of winglets on wind turbine blades using CFD.

[7] Hansen, T. H., & Mühle, F. (2018). Winglet optimization for a model-scale wind turbine. *Wind Energy*, *21*(8), 634-649.